Directed assembly of small binary clusters of magnetizable ellipsoids†

David H. Harris,[a] and Isaac Torres-Díaz[a*]

1 The magnetic field of a uniform magnetizable ellipsoid

The magnetic potential outside the magnetizable ellipsoidal particle ($\xi > 0$) generated by uniform magnetic field along the $x-$axis of the particle is[1]

$$\phi^+ = -xH_{0,x}\frac{\mu_m + (\mu_p-\mu_m)\frac{r_x r_y r_z}{2}\int_0^{\xi}\frac{d\alpha}{(\alpha+r_x^2)\sqrt{(\alpha+r_x^2)(\alpha+r_y^2)(\alpha+r_z^2)}}}{\mu_m + (\mu_p-\mu_m)\frac{r_x r_y r_z}{2}\int_0^{\infty}\frac{d\alpha}{(\alpha+r_x^2)\sqrt{(\alpha+r_x^2)(\alpha+r_y^2)(\alpha+r_z^2)}}}. \tag{1}$$

We define[2]

$$L_{r_j}(\xi) \equiv \int_0^{\xi} F_{r_j}(\lambda)d\lambda, \tag{2}$$

$$F_{r_j}(\lambda) = \frac{1}{\left(\lambda+r_j^2\right)\sqrt{\left(\lambda+r_x^2\right)\left(\lambda+r_y^2\right)\left(\lambda+r_z^2\right)}}. \tag{3}$$

The magnetic potential outside the magnetizable ellipsoidal particle (Eq. (1)) becomes

$$\phi^+ = -xH_{0,x}\frac{\mu_m + (\mu_p-\mu_m)\frac{r_x r_y r_z}{2}L_{r_j}(\xi)}{\mu_m + (\mu_p-\mu_m)\frac{r_x r_y r_z}{2}L_{r_j}(\infty)}. \tag{4}$$

Subtracting the magnetic potential of the uniform field $\phi_0 = (-xH_{0,x})$ along the $x-$axis of the particle, the disturbance potential generated by the particle results in

$$\phi = \phi^+ - \phi_0 = -xH_{0,x}\left(\frac{(\mu_p-\mu_m)\frac{r_x r_y r_z}{2}\left(L_{r_x}(\xi)-L_{r_x}(\infty)\right)}{\mu_m + (\mu_p-\mu_m)\frac{r_x r_y r_z}{2}L_{r_x}(\infty)}\right). \tag{5}$$

The disturbance magnetic field at position ξ outside the particle results equal to the negative gradient of the magnetic potential ϕ. The components of the magnetic field due to the magnetic field along the $x-$direction results

$$H_x = H_{0,x}\frac{(\mu_p-\mu_m)\frac{r_x r_y r_z}{2}\left(L_{r_x}(\xi)-L_{r_x}(\infty)\right)}{\mu_m + (\mu_p-\mu_m)\frac{r_x r_y r_z}{2}L_{r_x}(\infty)} + H_{0,x}x\frac{(\mu_p-\mu_m)\frac{r_x r_y r_z}{2}\frac{\partial L_{r_x}(\xi)}{\partial x}}{\mu_m + (\mu_p-\mu_m)\frac{r_x r_y r_z}{2}L_{r_x}(\infty)} \tag{6}$$

$$H_y = H_{0,x}x\frac{(\mu_p-\mu_m)\frac{r_x r_y r_z}{2}\frac{\partial L_{r_x}(\xi)}{\partial y}}{\mu_m + (\mu_p-\mu_m)\frac{r_x r_y r_z}{2}L_{r_x}(\infty)} \tag{7}$$

$$H_z = H_{0,x}x\frac{(\mu_p-\mu_m)\frac{r_x r_y r_z}{2}\frac{\partial L_{r_x}(\xi)}{\partial z}}{\mu_m + (\mu_p-\mu_m)\frac{r_x r_y r_z}{2}L_{r_x}(\infty)} \tag{8}$$

[a] Department of Chemical and Materials Engineering, The University of Alabama in Huntsville, Huntsville, AL 35899. Tel: +1-256-824-3596.
* Corresponding author: igd0002@uah.edu

Similarly, the disturbance magnetic field components due to the magnetic field along the $y-$direction results

$$H_x = H_{0,y} y \frac{(\mu_p-\mu_m)\frac{r_x r_y r_z}{2}\frac{\partial L_{r_y}(\xi)}{\partial x}}{\mu_m+(\mu_p-\mu_m)\frac{r_x r_y r_z}{2}L_{r_y}(\infty)} \tag{9}$$

$$H_y = H_{0,y}\frac{(\mu_p-\mu_m)\frac{r_x r_y r_z}{2}\left(L_{r_y}(\xi)-L_{r_y}(\infty)\right)}{\mu_m+(\mu_p-\mu_m)\frac{r_x r_y r_z}{2}L_{r_y}(\infty)} + H_{0,y} y \frac{(\mu_p-\mu_m)\frac{r_x r_y r_z}{2}\frac{\partial L_{r_y}(\xi)}{\partial y}}{\mu_m+(\mu_p-\mu_m)\frac{r_x r_y r_z}{2}L_{r_y}(\infty)} \tag{10}$$

$$H_z = H_{0,y} y \frac{(\mu_p-\mu_m)\frac{r_x r_y r_z}{2}\frac{\partial L_{r_y}(\xi)}{\partial z}}{\mu_m+(\mu_p-\mu_m)\frac{r_x r_y r_z}{2}L_{r_y}(\infty)} \tag{11}$$

The disturbance magnetic field components due to the magnetic field along the $z-$direction results,

$$H_x = H_{0,z} z \frac{(\mu_p-\mu_m)\frac{r_x r_y r_z}{2}\frac{\partial L_{r_z}(\xi)}{\partial x}}{\mu_m+(\mu_p-\mu_m)\frac{r_x r_y r_z}{2}L_{r_z}(\infty)} \tag{12}$$

$$H_y = H_{0,z} z \frac{(\mu_p-\mu_m)\frac{r_x r_y r_z}{2}\frac{\partial L_{r_z}(\xi)}{\partial y}}{\mu_m+(\mu_p-\mu_m)\frac{r_x r_y r_z}{2}L_{r_z}(\infty)} \tag{13}$$

$$H_z = H_{0,z}\frac{(\mu_p-\mu_m)\frac{r_x r_y r_z}{2}\left(L_{r_z}(\xi)-L_{r_z}(\infty)\right)}{\mu_m+(\mu_p-\mu_m)\frac{r_x r_y r_z}{2}L_{r_z}(\infty)} + H_{0,z} z \frac{(\mu_p-\mu_m)\frac{r_x r_y r_z}{2}\frac{\partial L_{r_z}(\xi)}{\partial z}}{\mu_m+(\mu_p-\mu_m)\frac{r_x r_y r_z}{2}L_{r_z}(\infty)} \tag{14}$$

Using the Clausius-Mossotti factor[3,4]

$$\mathfrak{f}_{jj} = \frac{1}{3}\frac{(\mu_p-\mu_m)}{\mu_m+(\mu_p-\mu_m)\frac{r_x r_y r_z}{2}L_{r_j}(\infty)}, \tag{15}$$

the disturbance magnetic field to the particle due to a magnetic field $\mathbf{H}_0 = (H_{0,x}, H_{0,y}, H_{0,z})$ in an arbitrary direction in the particle frame results

$$\begin{aligned} H_x = {} & \frac{3r_x r_y r_z}{2}\mathfrak{f}_{xx}\left[\left(L_{r_x}(\xi)-L_{r_x}(\infty)\right)+x\frac{\partial L_{r_x}(\xi)}{\partial x}\right]H_{0,x} \\ & + \frac{3r_x r_y r_z}{2}\mathfrak{f}_{yy}\left[y\frac{\partial L_{r_y}(\xi)}{\partial x}\right]H_{0,y} \\ & + \frac{3r_x r_y r_z}{2}\mathfrak{f}_{zz}\left[z\frac{\partial L_{r_z}(\xi)}{\partial x}\right]H_{0,z}, \end{aligned} \tag{16}$$

$$\begin{aligned} H_y = {} & \frac{3r_x r_y r_z}{2}\mathfrak{f}_{xx}\left[x\frac{\partial L_{r_x}(\xi)}{\partial y}\right]H_{0,x} \\ & + \frac{3r_x r_y r_z}{2}\mathfrak{f}_{yy}\left[\left(L_{r_y}(\xi)-L_{r_y}(\infty)\right)+y\frac{\partial L_{r_y}(\xi)}{\partial y}\right]H_{0,y} \\ & + \frac{3r_x r_y r_z}{2}\mathfrak{f}_{zz}\left[z\frac{\partial L_{r_z}(\xi)}{\partial y}\right]H_{0,z}, \end{aligned} \tag{17}$$

$$
\begin{aligned}
H_z &= \frac{3r_x r_y r_z}{2}\mathfrak{f}_{xx}\left[x\frac{\partial L_{r_x}(\xi)}{\partial z}\right]H_{0,x} \\
&\quad + \frac{3r_x r_y r_z}{2}\mathfrak{f}_{yy}\left[y\frac{\partial L_{r_y}(\xi)}{\partial z}\right]H_{0,y} \\
&\quad + \frac{3r_x r_y r_z}{2}\mathfrak{f}_{zz}\left[\left(L_{r_z}(\xi)-L_{r_z}(\infty)\right)+z\frac{\partial L_{r_z}(\xi)}{\partial z}\right]H_{0,z}. \qquad (18)
\end{aligned}
$$

Thus, the disturbance field outside the ellipsoidal particle under the influence of arbitrarily oriented uniform magnetic field $\mathbf{H}_0$ can be expressed as

$$
\mathbf{H} = \frac{3r_x r_y r_z}{2}\mathscr{G}\cdot\mathfrak{f}\cdot\mathbf{H}_0, \qquad (19)
$$

where $\mathscr{G}$ is a tensor, which is equivalent to the Green tensor in ellipsoidal coordinates with components

$$
\mathscr{G}_{ij} = \delta_{ij}\left[L_{r_j}(\xi)-L_{r_j}(\infty)\right]+x_j\frac{\partial L_{r_j}(\xi)}{\partial x_i}, \qquad (20)
$$

where δ_{ij} represents the identity tensor and L_{r_j} is a scalar function. Additionally, $\frac{\partial L_{r_j}(\xi)}{\partial x_i} = \frac{\partial L_{r_j}(\xi)}{\partial \xi}\frac{\partial \xi}{\partial x_i}$, and

$$
\begin{aligned}
\frac{\partial L_{r_j}(\xi)}{\partial \xi} &= F_{r_j}(\xi), \qquad (21) \\
\frac{\partial \xi}{\partial x_i} &= \frac{2x_i}{(r_i^2+\xi)}\Big/\left(\frac{x^2}{(r_x^2+\xi)^2}+\frac{y^2}{(r_y^2+\xi)^2}+\frac{z^2}{(r_z^2+\xi)^2}\right). \qquad (22)
\end{aligned}
$$

2 Number of particles

Figure S1 shows representative snapshots of MC simulations for the directed assembly of binary suspensions composed of paramagnetic spheres $\tilde{r}^P = 5$ and diamagnetic ellipsoids $\tilde{r}_x^D/\tilde{r}_y^D = 5$. The simulation results in Figure 1 have a fixed area fraction $\phi = 0.1$, but a different number ratio between diamagnetic and paramagnetic particles (N_D/N_P). Figure S1 shows that the simulations require a large number ratio N_D/N_P between particles to guarantee a predicted equilibrium structure around the paramagnetic particle. We use the number ratio between particles $N_D/N_P = 100$ to analyze the directed assembly of binary suspensions when one of the components is dilute with respect to the other component.

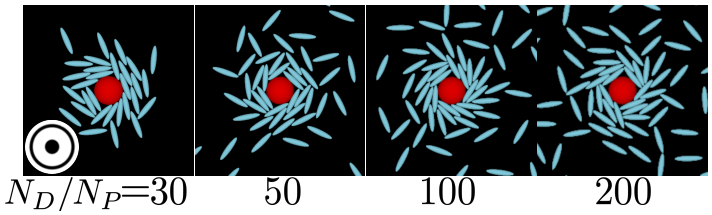

Fig. S 1 Snapshots of MC simulations of binary suspensions of a paramagnetic (P) particle in red and diamagnetic (D) particles in cyan with different number ratio N_D/N_P between particles. The binary suspensions have an area fraction $\phi = 0.1$ and a dipole-field interaction parameter $\alpha_s = 10^4$. The aspect ratio of the sphere is $\tilde{r}^P = 5$ and the ellipsoid is $\tilde{r}_x^D/\tilde{r}_y^D = 5$. The medium permeabilities is $\mu_m/\mu_0 = 1.04$.

3 Model validation - parameters

	$\mu_0 H_0$		
μ_m/μ_0	6 gauss	12 gauss	60 gauss
1.0054 - 1.2157	101, 267.0105	101, 267.0105	101, 267.0105

Table 1 Number of particles and simulation box length $(N, L_{box}/r_m)$ used in Figures 5.

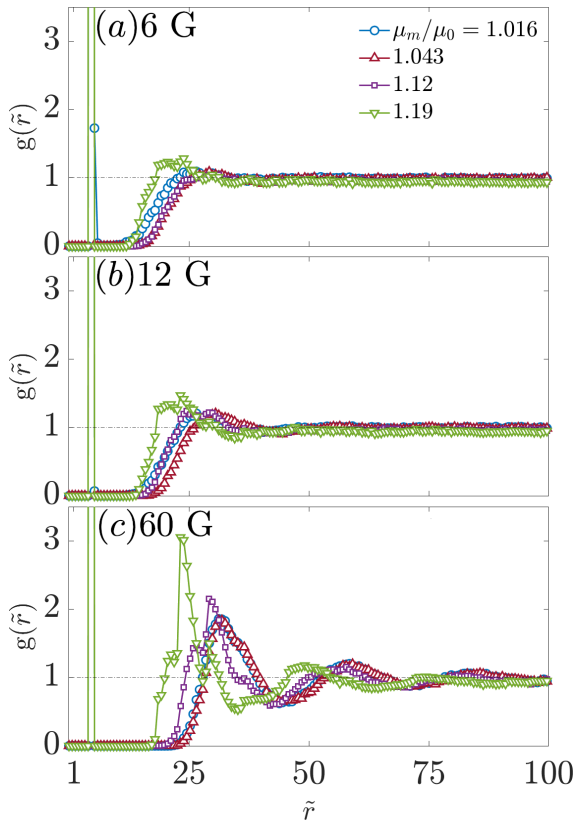

Fig. S 2 Radial distribution function $g(\tilde{r})$ between the central diamagnetic particle $(\tilde{r}^D = 3.67)$ and surrounding paramagnetic particles $(\tilde{r}^P = 1)$ shown in Figure 5 as a function of medium permeability and at different applied magnetic fields $\mu_0 H_0$ of (a) 6, (b) 12, and (c) 60 gauss. The results corresponds with Figure 5 in the main document.

4 Simulation conditions

	μ_m/μ_0			
$\tilde{r}_x^D/\tilde{r}_y^D$	1.04	1.11	1.19	1.26
9	101, 58.39	101, 58.39	101, 58.39	101, 58.39
6	101, 57.90	101, 57.90	101, 57.90	101, 57.90
3	101, 56.81	101, 56.81	101, 56.81	101, 56.81
1	101, 56.46	101, 56.46	101, 56.46	101, 56.46

Table 2 Number of particles and simulation box length $(N, L_{box}/r_m)$ used in Figures 6 – 7.

	μ_m/μ_0			
$\tilde{r}_x^D/\tilde{r}_y^D$	1.04	1.11	1.19	1.26
5	101, 128.56	101, 128.56	101, 128.56	101, 128.56
4	101, 114.94	101, 114.94	101, 114.94	101, 114.94
3	101, 100.10	101, 100.10	101, 100.10	101, 100.10
2	101, 84.067	101, 84.067	101, 84.067	101, 84.067
1	201, 84.450	101, 62.110	101, 62.110	101, 62.110

Table 3 Number of particles and simulation box length $(N, L_{box}/r_m)$ used in Figures 8 – 9.

	$\tilde{r}_x^P/\tilde{r}_y^P$				
$\tilde{r}_x^D/\tilde{r}_y^D$	1	2	3	4	5
8	101, 158.60	101, 158.30	90, 151.19	90, 150.72	90, 151.83
6	101, 137.28	101, 137.78	101, 137.93	101, 138.69	101, 140.05
5	101, 124.97	101, 125.33	101, 126.48	101, 127.13	101, 128.56
4	101, 111.69	101, 112.33	101, 112.93	101, 113.79	100, 114.94
3	101, 97.21	101, 98.10	101, 98.24	101, 99.59	100, 100.10
2	101, 79.38	101, 79.67	101, 81.20	101, 82.04	100, 84.07

Table 4 Number of particles and simulation box length $(N, L_{box}/r_m)$ used in Figures 10 – 11.

	$\tilde{r}_x^P/\tilde{r}_y^P$				
$\tilde{r}_x^D/\tilde{r}_y^D$	1	2	3	4	5
8	101, 158.60	101, 158.30	90, 151.19	90, 150.72	90, 151.83
6	101, 137.28	101, 137.77	101, 137.93	101, 138.69	101, 140.05
5	101, 124.97	101, 125.33	101, 126.48	101, 127.13	101, 128.56
4	101, 111.69	101, 112.33	101, 112.93	101, 113.79	100, 114.94
3	101, 97.21	101, 98.08	101, 98.24	101, 99.59	100, 100.10
2	101, 79.38	101, 79.67	101, 81.20	101, 82.04	100 , 84.07

Table 5 Number of particles and simulation box length $(N, L_{box}/r_m)$ used in Figures 12 – 13.

5 Simulation results - Effect of dipolar interactions

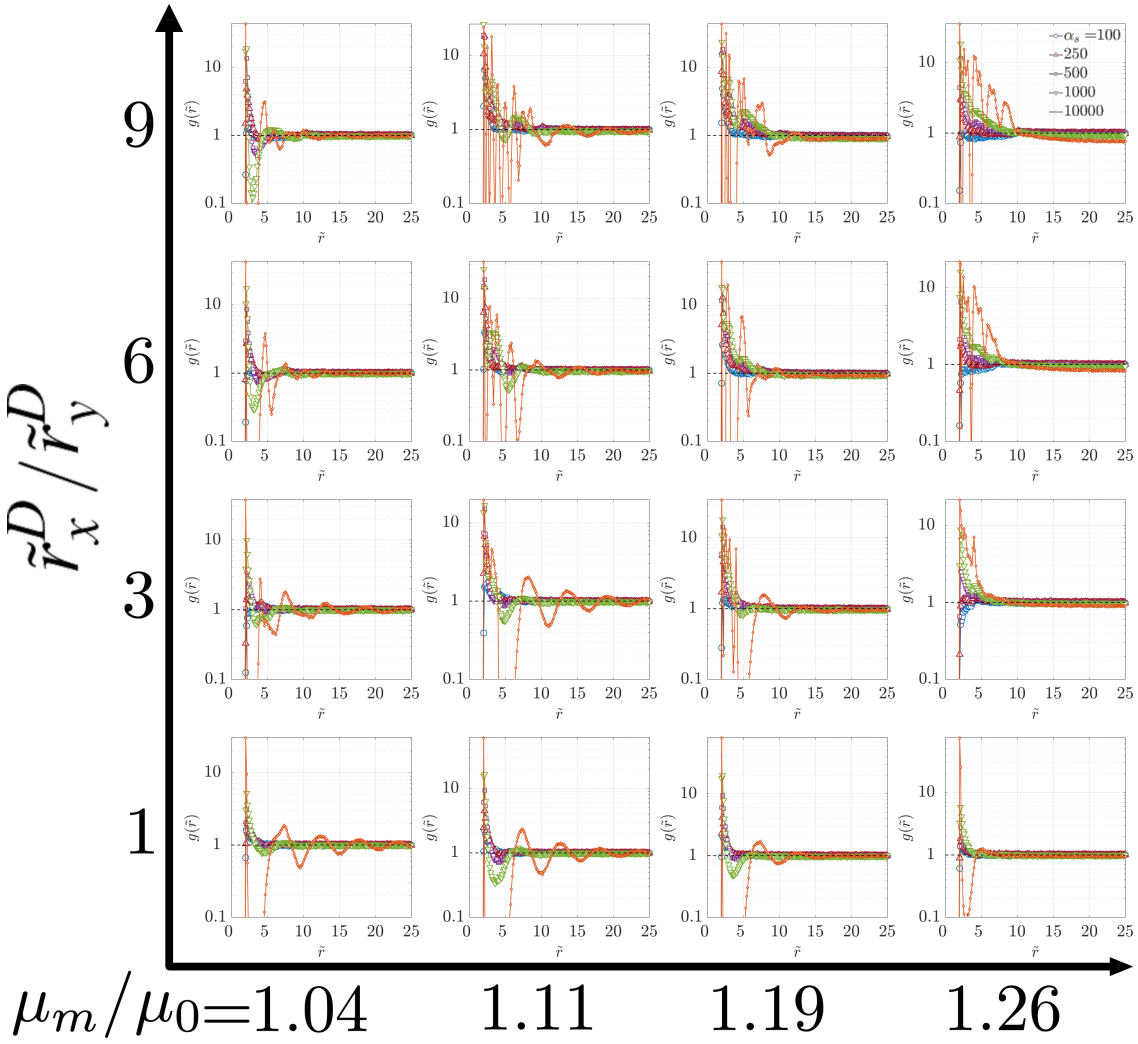

Fig. S 3 Radial distribution function $g(\tilde{r})$ between the central diamagnetic ellipsoid $(\tilde{r}_x^D/\tilde{r}_y^D)$ and surrounding paramagnetic spheres $(\tilde{r}^P = 1)$ for different dipole-field interaction parameters α_s. The results corresponds with Figure 6 in the main document.

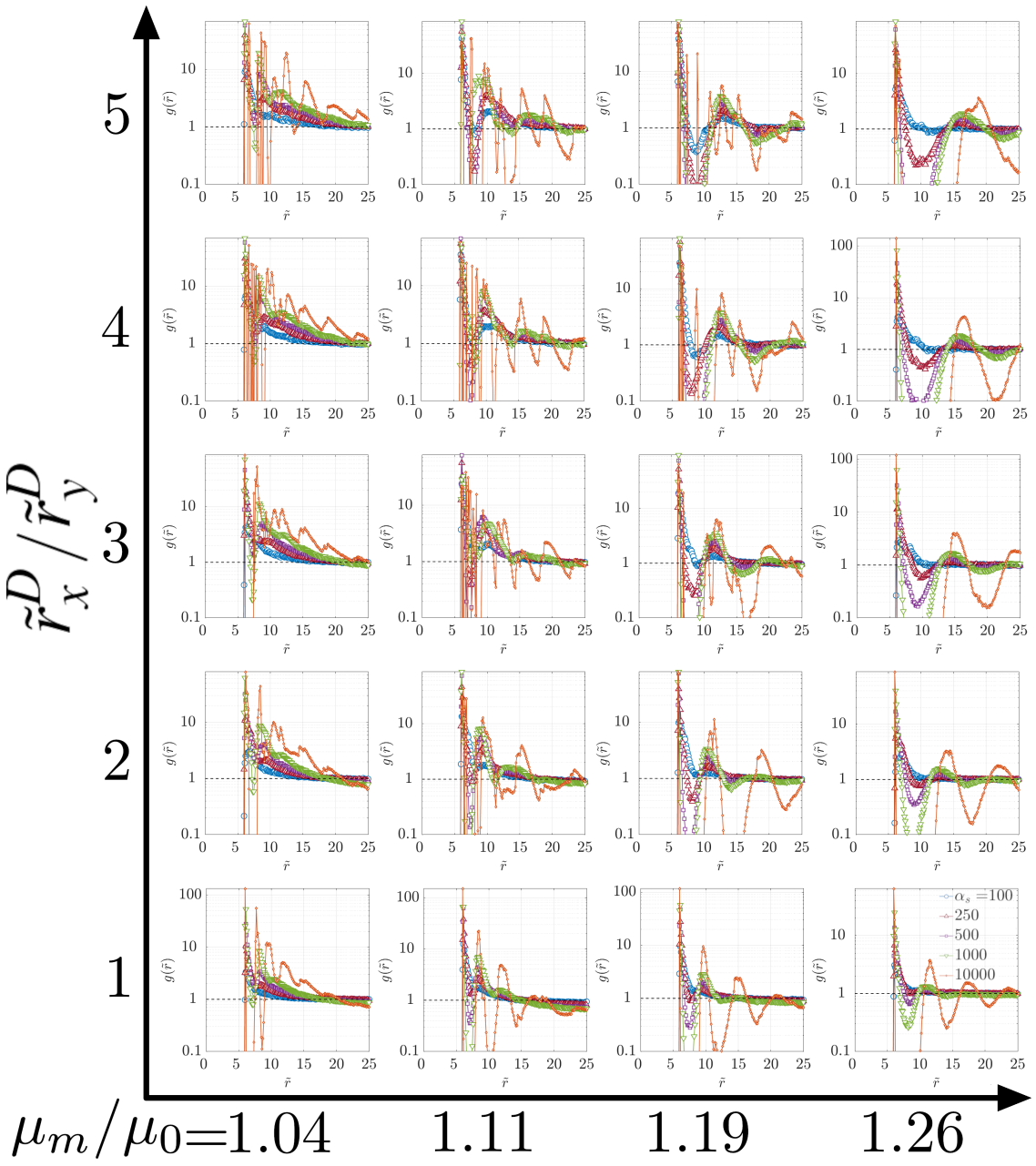

Fig. S 4 Radial distribution function $g(\tilde{r})$ between the central paramagnetic sphere ($\tilde{r}^P = 5$) and surrounding diamagnetic ellipsoids with different aspect ratios $\tilde{r}_x^D/\tilde{r}_y^D$ for different dipole-field interaction parameters α_s. The results corresponds with Figure 7 in the main document.

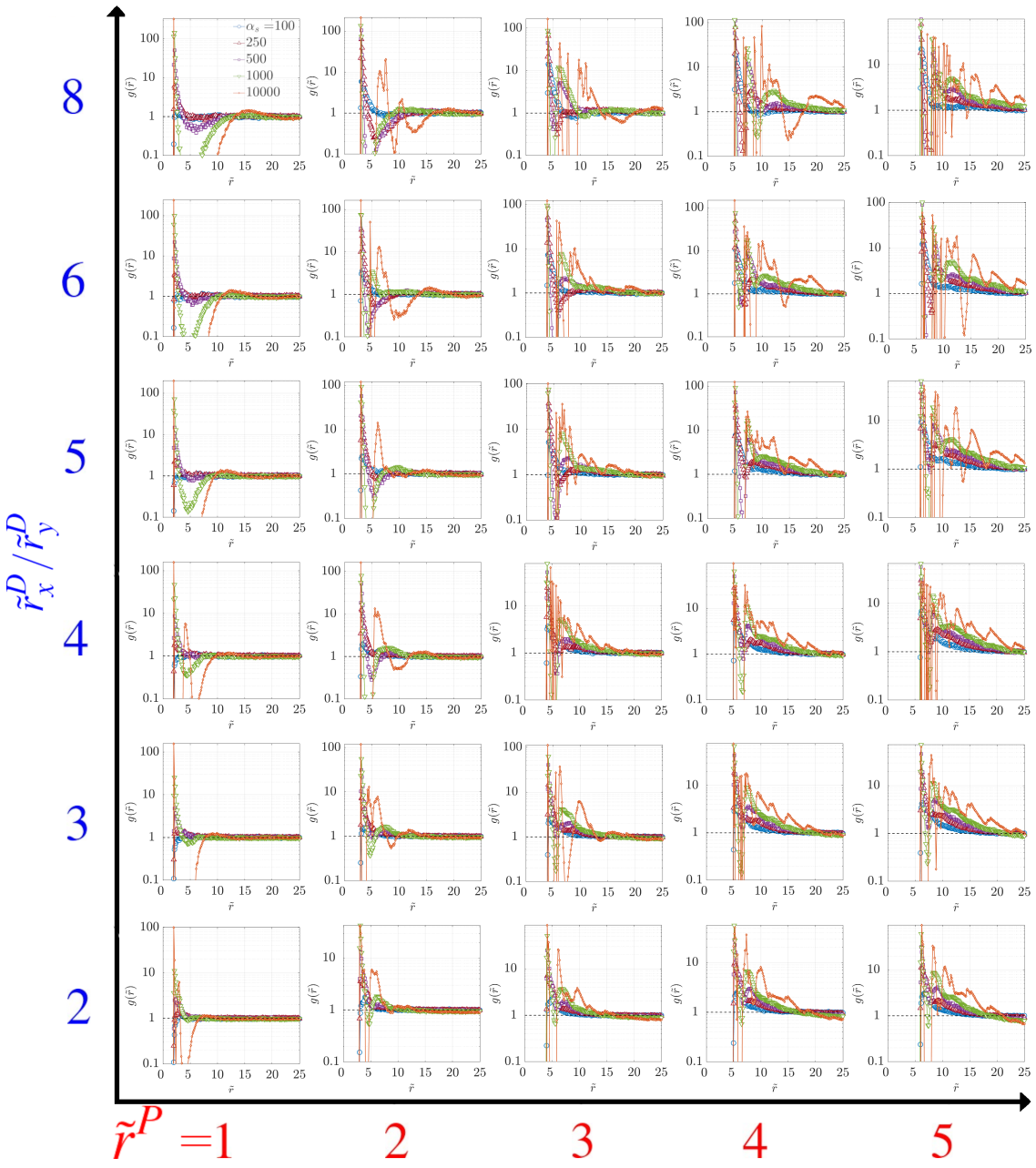

Fig. S 5 Radial distribution function $g(\tilde{r})$ between the central paramagnetic sphere with radius $\tilde{r}^P$ and diamagnetic ellipsoids with different aspect ratios $\tilde{r}_x^D/\tilde{r}_y^D$ for different dipole-field interaction parameters α_s. The results corresponds with Figure 8 in the main document.

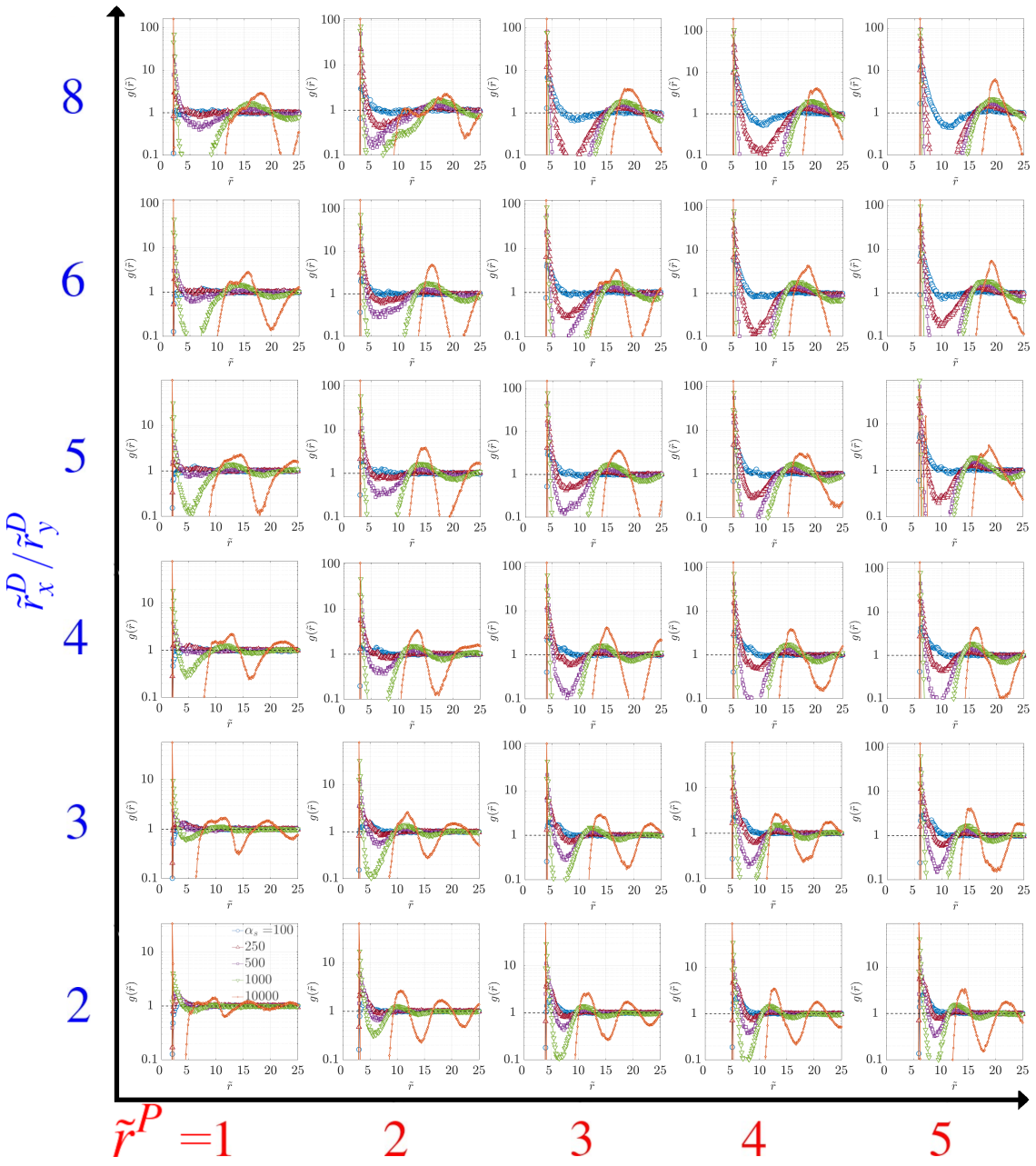

Fig. S 6 Radial distribution function $g(\tilde{r})$ between the central paramagnetic sphere with radius $\tilde{r}^P$ and diamagnetic ellipsoids with different aspect ratios $\tilde{r}_x^D/\tilde{r}_y^D$ for different dipole-field interaction parameters α_s. The results corresponds with Figure 9 in the main document.

Figure S7 shows representative snapshots of MC simulations of the directed assembly of binary suspensions with a paramagnetic sphere and diamagnetic ellipsoids as a function of relative permeabilities μ_P/μ_0, μ_P/μ_m, μ_D/μ_m, and α_s.

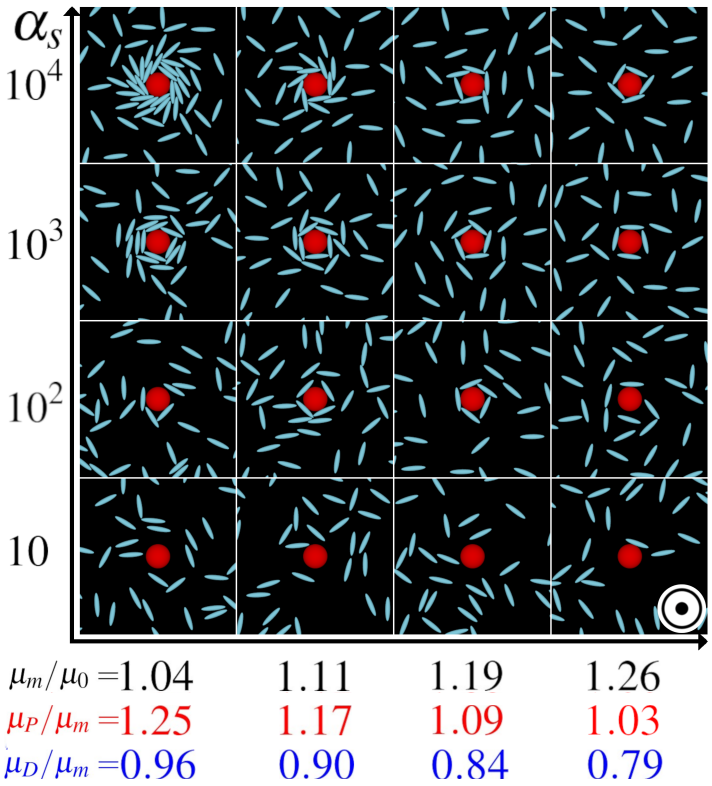

Fig. S 7 Snapshots of MC simulations of the assembly of binary mixtures composed of a paramagnetic sphere (red) ($\tilde{r}^P = 5$) and diamagnetic ellipsoids (cyan) ($\tilde{r}_x^D/\tilde{r}_y^D = 5$) as a function of relative permeability and α_s. The magnetic field is directed perpendicular to the assembly plane.

Notes and references

1 J. A. Stratton, *Electromagnetic Theory*, McGraw-Hill Book Company, Inc., New York, 1941, p. 615.

2 T. Thelen, A. Jara and I. Torres-Díaz, *Soft Matter*, 2023, **19**, 640–651.

3 T. B. Jones, *Electromechanics of Particles*, Cambridge University Press, 1995.

4 H. Morgan and N. G. Green, *AC electrokinetics : colloids and nanoparticles*, Institute of Physics Pub., Philadelphia, Pa., 2003.